

WASP-12b: THE HOTTEST TRANSITING EXTRASOLAR PLANET YET DISCOVERED

L. HEBB¹, A. COLLIER-CAMERON¹, B. LOELLET², D. POLLACCO³, G. HÉBRARD⁴, R. A. STREET⁵, F. BOUCHY^{4,6}, H. C. STEMPELS¹, C. MOUTOU², E. SIMPSON³, S. UDRY⁷, Y. C. JOSHI³, R. G. WEST⁸, I. SKILLEN⁹, D. M. WILSON¹⁰, I. McDONALD¹⁰, N. P. GIBSON³, S. AIGRAIN¹¹, D. R. ANDERSON¹⁰, C. R. BENN⁹, D. J. CHRISTIAN³, B. ENOCH¹, C. A. HASWELL¹², C. HELLIER¹⁰, K. HORNE¹, J. IRWIN¹³, T. A. LISTER⁵, P. MAXTED¹⁰, M. MAYOR⁷, A. J. NORTON¹², N. PARLEY¹, F. PONT¹¹, D. QUELOZ⁷, B. SMALLEY¹⁰, AND P. J. WHEATLEY¹⁴

¹ School of Physics and Astronomy, University of St. Andrews, North Haugh, St. Andrews, Fife, KY16 9SS, UK

² Laboratoire d’Astrophysique de Marseille, BP 8, 13376 Marseille Cedex 12, France

³ Astrophysics Research Centre, School of Mathematics & Physics, Queen’s University, University Road, Belfast, BT7 1NN, UK

⁴ Institut d’Astrophysique de Paris, CNRS (UMR 7095), Université Pierre & Marie Curie, 98^{bis} bd. Arago, 75014 Paris, France

⁵ Las Cumbres Observatory, 6740 Cortona Dr. Suite 102, Santa Barbara, CA 93117, USA

⁶ Observatoire de Haute-Provence, 04870 St. Michel l’Observatoire, France

⁷ Observatoire de Genève, Université de Genève, 51 Ch. des Maillettes, 1290 Sauverny, Switzerland

⁸ Department of Physics and Astronomy, University of Leicester, Leicester, LE1 7RH, UK

⁹ Isaac Newton Group of Telescopes, Apartado de Correos 321, E-38700 Santa Cruz de la Palma, Tenerife, Spain

¹⁰ Astrophysics Group, Keele University, Staffordshire, ST5 5BG, UK

¹¹ School of Physics, University of Exeter, EX4 4QL, UK

¹² Department of Physics and Astronomy, The Open University, Milton Keynes, MK7 6AA, UK

¹³ Harvard-Smithsonian Center for Astrophysics, 60 Garden Street, Cambridge, MA 02138, USA

¹⁴ Department of Physics, University of Warwick, Coventry, CV4 7AL, UK

Received 2008 September 10; accepted 2008 December 15; published 2009 March 10

ABSTRACT

We report on the discovery of WASP-12b, a new transiting extrasolar planet with $R_{\text{pl}} = 1.79^{+0.09}_{-0.09} R_J$ and $M_{\text{pl}} = 1.41^{+0.10}_{-0.10} M_J$. The planet and host star properties were derived from a Monte Carlo Markov chain analysis of the transit photometry and radial velocity data. Furthermore, by comparing the stellar spectrum with theoretical spectra and stellar evolution models, we determined that the host star is a supersolar metallicity ($[M/H] = 0.3^{+0.05}_{-0.15}$), late-F ($T_{\text{eff}} = 6300^{+200}_{-100}$ K) star which is evolving off the zero-age main sequence. The planet has an equilibrium temperature of $T_{\text{eq}} = 2516$ K caused by its very short period orbit ($P = 1.09$ days) around the hot, twelfth magnitude host star. WASP-12b has the largest radius of any transiting planet yet detected. It is also the most heavily irradiated and the shortest period planet in the literature.

Key words: planetary systems – techniques: photometric – techniques: radial velocities

1. INTRODUCTION

Transiting extrasolar planets have provided tremendous information about the properties of planets outside our solar system. Since 2006, a burst of new planet discoveries has been reported. We are now beginning to see the variety of exoplanets which exist in the Galaxy and to classify them based on their properties. Furthermore, due to the increasing number of planets being discovered and due to the detailed, multiwavelength follow-up of a handful of very bright transiting systems (e.g., HD 209458, HD 189733), we are able to provide strong observational tests of theoretical models of planet formation and evolution.

Exotic planets are particularly important because they push the boundaries of our theoretical understanding. HD 209458b, for example, confounded theorists with its large radius (Brown et al. 2001). Since its discovery, a class of similar planets has been found suggesting that these highly irradiated, low-density planets are not rare. Here, we report on the discovery of a new extreme transiting extrasolar planet with a short orbital period, enlarged radius, and supersolar metallicity host star.

In this paper, we first describe all the observations we obtained to detect and analyze the transiting star–planet system (Section 2). We describe the data analysis in Section 3 where we present the properties of the planet and its host star. Finally in Section 4, we discuss the planet properties in the context of current theoretical understanding of planet formation.

2. OBSERVATIONS

2MASS J063032.79+294020.4 (hereafter WASP-12) is a bright F9V star. It has been identified in several northern sky catalogs which provide broadband optical (Zacharias et al. 2004) and infrared Two Micron All Sky Survey (2MASS) magnitudes (Skrutskie et al. 2006) and proper-motion information. Coordinates and broadband magnitudes of the star are given in Table 1.

2.1. SuperWASP Photometry

Time-series photometry of WASP-12 was obtained in the 2004 and 2006 seasons with the SuperWASP-N camera located on La Palma, Canary Islands (Pollacco et al. 2006). In 2004, when the target was first observed, only 820 photometric measurements were obtained between 2004 August and 2004 September. However, the same fields were observed again in 2006 after upgrades to the telescope mount and instrument. During the 2006 season, the target was observed in the field of view (FOV) of two separate cameras, and a total of 5573 photometric brightness measurements were obtained between 2006 November and 2007 March. The data obtained in both seasons were processed with a custom-built data reduction pipeline described in Pollacco et al. (2006), and the resulting light curves were analyzed using a modified box least-squares algorithm (Collier Cameron et al. 2006; Kovcs et al. 2002) to search for the planetary transit signature.

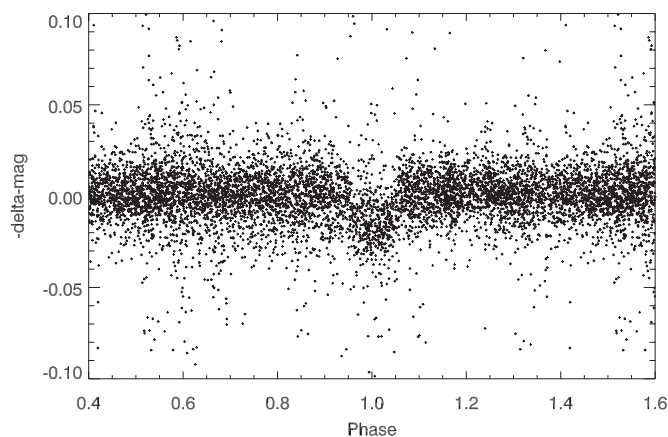


Figure 1. SuperWASP discovery light curve of WASP-12 phase-folded with a period, $P = 1.09142$ days and epoch, $T_0 = 2454476.2321$.

Table 1
Stellar Parameters for WASP-12^a

Parameter	WASP-12
R.A.(J2000)	06:30:32.79
Decl.(J2000)	+29:40:20.4
B	12.11 ± 0.08
V	11.69 ± 0.08
I	11.03 ± 0.08
J	10.477 ± 0.021
H	10.228 ± 0.022
K	10.188 ± 0.020
T_{eff}	6300^{+200}_{-100} K
[M/H]	$0.30^{+0.05}_{-0.15}$
$\log g$	4.38 ± 0.10
$v \sin i$	$< 2.2 \pm 1.5$ km s ⁻¹

Notes. ^a The broadband magnitudes are obtained from the NOMAD 1.0 Catalog. The stellar parameters are derived from our spectral synthesis of observed spectra of WASP-12 (see Section 3.1).

The combined SuperWASP data showed a significant periodic dip in brightness with a period, $P = 1.091$ days, duration, $\tau \sim 2.7$ hr, and depth, $\delta \sim 14$ mmag. The improvement in χ^2 of the box-shaped transit model over the flat light curve was $\delta\chi^2 = 719$ and the signal-to-red noise (Pont et al. 2006) was $\text{SN}_{\text{red}} = 15.6$. A total of 23 partial or full transits were captured by SuperWASP.

There were no obvious objects blended with WASP-12 in the SuperWASP aperture, and the detected transit event was significant, therefore, WASP-12 was classed as a high priority target needing further study. In Figure 1, we show the phase-folded light curve of the SuperWASP data, adopting the ephemeris resulting from the box least-squares analysis on the combined light curve.

2.2. Follow-up Multiband Photometry

After identification as a high-priority transit candidate, the follow-up photometry of WASP-12 was obtained using two additional telescopes with high spatial resolution (less than $1''$ pixel⁻¹) compared to SuperWASP ($13''.7$ pixel⁻¹). We obtained observations of WASP-12 and the surrounding region during the predicted time of transit to confirm that there are no eclipsing binaries within 1 arcminute of WASP-12 that may have caused the transit signal in the SuperWASP data. WASP-

12 also appears to be a single star at the resolution provided by these data. The closest companion is $9''$ from the target and has a magnitude of $V \sim 18$. Encouraged by this, we then obtained complete B , I , and z -band light curves of the transit. A detailed description of the follow-up photometry is given below.

2.2.1. Tenagra Telescope Photometry

WASP-12 was observed using the fully robotic, Tenagra II, 0.81 m f/7 Ritchey–Chrétien telescope sited in Arizona, USA. The science camera contains a $1\text{k} \times 1\text{k}$ SITe CCD with a pixel scale of $0''.87$ pixel⁻¹ and an FOV of $14''.8 \times 14''.8$. These photometric data were obtained as part of an observing program sponsored by the Las Cumbres Observatory Global Telescope Network.¹⁵ The B -band transit of WASP-12 was created from 227 observations taken on two consecutive nights in March. The I -band light curve consists of 639 flux measurements taken over five nonphotometric nights in 2008 February and March.

Calibration frames obtained automatically every twilight were used in processing the images (bias subtraction and flat fielding) with the SuperWASP data reduction pipeline (Pollacco et al. 2006). Object detection and aperture photometry, with a 7.5 pixel radius aperture, were performed on all the stars in the frame using DAOPHOT (Stetson 1987) run under IRAF.¹⁶ The differential photometry was derived from seven, nonvariable comparison stars within the field which had $V < 14$ magnitude and $J-H$ colors similar to the target star. For each of the filters, the fluxes from the comparison stars were summed, and then converted into a magnitude which was then subtracted from the instrumental magnitude of the target star. The resulting differential photometry of the B -band light curve has an rms of ~ 7 mmag.

The I -band transit was created from data obtained in nonphotometric conditions over five different visits to the star (some at high air mass). These data were essential in confirming the transit and refining the ephemeris, but show significant red noise systematics. Therefore, they were unsuitable for defining accurate transit parameters and were excluded when modeling the light curve.

2.2.2. Liverpool Telescope Photometry

A full transit was observed using RATCam on the robotic 2 m Liverpool Telescope (LT; Steele et al. 2004) on La Palma as part of the Canarian Observatories International Time Programme. A total of 614 images were taken in the Sloan z' band on the night of 2008 February 18. We employed 2×2 binning ($0''.27$ pixel⁻¹) and used a 10 s exposure time for all observations. The night was photometric, and the pointing was stable. The target star did not drift more than a few pixels throughout the transit which allowed for very accurate differential photometry.

The images were debiased, flat-fielded, and corrected for fringing using the standard RATCAM processing pipeline.¹⁷ IRAF DAOPHOT was then used to obtain aperture photometry of the target and four, nonvariable nearby comparison stars using a 15 pixel radius aperture. The comparison stars were chosen primarily for brightness from within the limited FOV ($4''.6 \times 4''.6$) of the camera and are not necessarily matched in color to the target. The differential photometry was performed

¹⁵ <http://www.lcogt.net>

¹⁶ IRAF is distributed by the National Optical Astronomy Observatories, which is operated by the Association of Universities for Research in Astronomy, Inc., under cooperative agreement with the National Science Foundation.

¹⁷ See <http://telescope.livjm.ac.uk/Info/TelInst/Inst/RATCam/>.

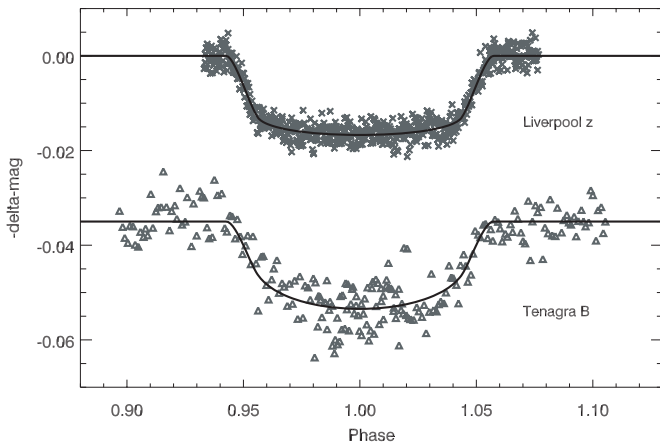


Figure 2. Differential z -band (top) and Tenagra B -band (bottom) photometry of WASP-12 during the transit. An offset has been added to the B -band data for clarity. The data are phase-folded with the ephemeris given in Table 3. Overplotted are the best-fit model transit light curves using the formalism of Mandel & Agol (2002) applying the limb darkening coeffs from Claret (2000, 2004).

in the same way as described above for the Tenagra data, and the resulting out-of-eclipse light curve has 2.5 mmag precision. The z -band and B -band transit light curves obtained via follow-up photometry are plotted in Figure 2.

2.3. SOPHIE Spectroscopy

High-resolution spectroscopy of WASP-12 was obtained between 2008 February 12–22 with the SOPHIE spectrograph (Bouchy The Sophie Team 2006) on the 1.93 m telescope at the Observatoire de Haute Provence. We used the same observing program and instrument setup as for other SuperWASP planets discovered in the northern hemisphere (Pollacco et al. 2008; Christian et al. 2009; West et al. 2008).

The weather was clear and reasonably stable throughout the run, although there were some fluctuations in seeing and transparency. Therefore, we adopted exposure times of 900 s and 1080 s depending on the transparency. This allowed us to achieve a signal-to-noise (S/N) per resolution element (at 5500 Å) of 30–45 in all the spectra. The S/N values for all the spectra are listed in Table 2. The spectra were processed in real time with the SOPHIE instrument control and data reduction software, and the radial velocity (RV) measurements were obtained using a weighted cross-correlation method (Baranne et al. 1996; Pepe et al. 2005). To do this, we used a numerical mask constructed from the solar spectrum atlas corresponding to a G2V star.

The Moon was bright over most of the run thus contaminating the spectra with scattered light. We removed its velocity signature (according to the procedure described in Pollacco et al. 2008) from all the spectra. We then fit the resulting cross-correlation function from each spectrum with a Gaussian to derive a value for the central RV, the FWHM (10.15–10.30 km s⁻¹), and the peak amplitude or contrast (28.60%–29.44%). The uncertainties for all RV measurements were derived using an empirical relation applicable to SOPHIE spectra taken in the high efficiency mode (West et al. 2008; F. Bouchy et al. 2009, in preparation).

In this way, we obtained 21 RV measurements of WASP-12 over 10 nights which have typical uncertainties of ~ 10 m s⁻¹. The RV measurement obtained from each spectrum is listed in Table 2 along with the derived uncertainty. These data have a standard deviation of 130 m s⁻¹, signifi-

Table 2
The RV Measurements of WASP-12 Obtained with SOPHIE Spectrograph

BJD	V_r (km s ⁻¹)	σ_{RV} (km s ⁻¹)	S/N	Bisector (km s ⁻¹)
2454509.38633	18.9231	0.0088	44.3	0.015
2454509.53836	19.0845	0.0112	34.9	0.047
2454510.40255	18.8497	0.0102	38.0	0.046
2454511.29105	18.9394	0.0082	47.4	0.056
2454511.36791	18.9008	0.0090	43.0	0.047
2454511.40825	18.8582	0.0090	43.3	0.047
2454511.53661	18.8945	0.0108	36.1	0.005
2454512.28835	19.0648	0.0088	44.0	0.057
2454512.30278	19.0429	0.0084	45.6	0.031
2454512.31570	19.0298	0.0096	40.1	0.010
2454512.32867	19.0064	0.0090	42.7	0.033
2454512.34174	18.9973	0.0088	44.2	0.030
2454512.35470	18.9778	0.0086	45.2	0.036
2454512.40579	18.9176	0.0090	42.6	0.038
2454512.43225	18.9124	0.0088	44.4	0.047
2454512.44721	18.8936	0.0086	45.6	0.018
2454513.32972	19.0957	0.0128	29.7	0.079
2454514.30357	19.2105	0.0130	29.6	-0.001
2454515.27220	19.3213	0.0106	36.1	-0.018
2454516.40210	19.2961	0.0128	29.8	0.067
2454519.43071	19.1968	0.0088	44.3	0.038

cantly greater than the individual uncertainties, and they vary sinusoidally when folded on the period derived from the transit photometry (Figure 4).

Finally, any asymmetries in the line profiles were explored by measuring the velocity span of the line bisector (Gray 1988) according to the technique outlined in Queloz et al. (2001). These measurements, also listed in Table 2, show no correlation with RV (Figure 3), therefore it is unlikely that the observed RV variations are caused by star spots on the stellar surface or by blending with an eclipsing binary star in the system or close to the line of sight (LOS).

Thus, we conclude that the observed RV variations are caused by the gravitational influence of a planetary-mass object orbiting WASP-12. Figure 4 shows a plot of the RV measurements phase-folded on the ephemeris given in Table 3 and overplotted with the best-fitting model RV curve which is derived as described in the analysis section (Section 3.2).

2.4. Additional Spectroscopy

The SOPHIE spectra were obtained in the high-efficiency (HE) mode which is known to suffer from problems with corrections for the blaze shape. According to the data products Web site, a residual blaze effect remains in the reduced spectra at the 5% level.¹⁸ These data provide exceptional RV precision, but they are not always suitable for determining stellar parameters. For example, the effective temperature is strongly constrained by the wings of the H α line, and for hot stars with broad H α wings, the residual instrumental features in the SOPHIE HE spectra lead to large uncertainties on this parameter. Therefore, in addition to the 21 SOPHIE spectra which were used primarily to measure the velocity signature of the orbiting planet, several additional spectra of WASP-12 were obtained and used in deriving independent measurements of the stellar parameters of the host star. The additional spectroscopic observations are described below, and the derivation of

¹⁸ See http://www.obs-hp.fr/www/guide/sophie/data_products.html.

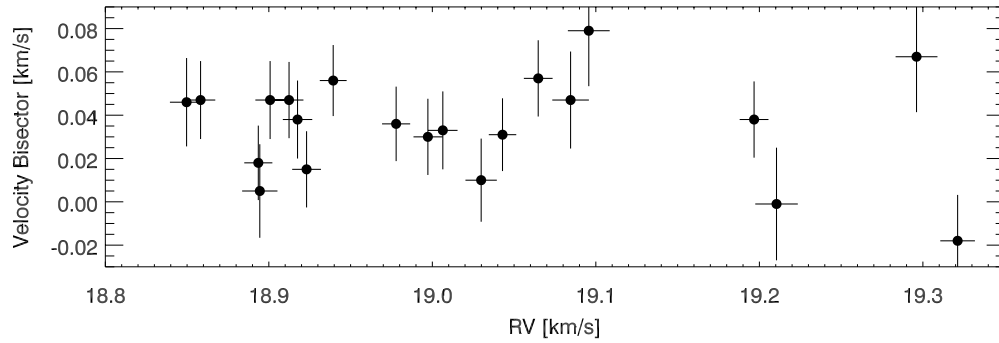


Figure 3. Line-bisector velocity vs. RV measured from all the observed SOPHIE spectra. We adopt uncertainties of twice the RV uncertainty for all bisector measurements. There is no correlation between these two parameters indicating that the RV variations are not caused by stellar activity or LOS binarity.

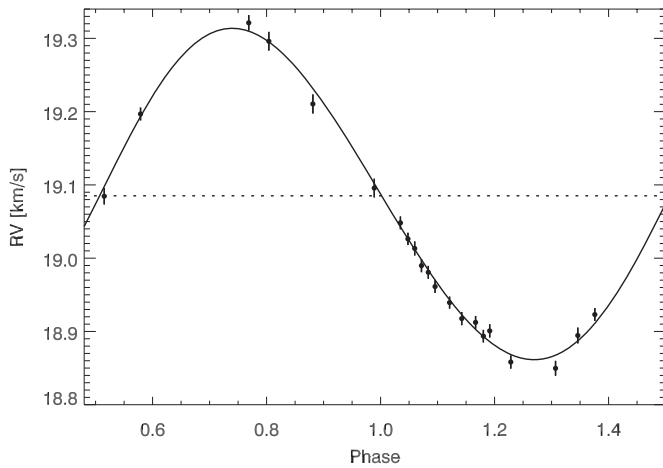


Figure 4. SOPHIE RV curve of WASP-12 phase-folded with the ephemeris given in Table 3. The solid line is the best model curve resulting from the orbital parameters of the system derived from the MCMC analysis in Section 3.2. The systemic RV value is shown by the dotted line.

the stellar parameters from all available spectra are described in Section 3.1.

2.4.1. Isaac Newton Telescope Spectra

Two individual spectra of WASP-12 were obtained on 2008 April 22 with the 2.5 m Isaac Newton Telescope and Intermediate Dispersion Spectrograph (IDS). The long-slit data were taken with the H1800V grating using a $1/2$ slit which resulted in a resolution of ($R \sim 8000$). An S/N of greater than 50 was achieved in both individual spectra by taking 900 s exposures. The spectrum was centered at 6500 \AA and covered the region from 6200 to 7000 \AA , thereby providing measurements of $H\alpha$, the Li I doublet at 6708 \AA , and many narrow metal lines. Biases and lamp flats were obtained at the beginning of the night and neon-copper-argon arcs were taken just before and just after the WASP-12 observations. The spectra were reduced in a standard way using the IRAF *longslit* package. We then averaged the two individual spectra and continuum normalized the composite observation before fitting for the stellar parameters.

2.4.2. Telescopio Nazionale Galileo Spectra

We observed the target again on 2008 April 29 using the high-efficiency echelle spectrograph, SARG, mounted on the 3.58 m Telescopio Nazionale Galileo (TNG) telescope. These data were

Table 3
WASP-12 System Parameters and 1σ Error Limits Derived from the MCMC Analysis

Parameter	Symbol	Value	Units
Transit Epoch (BJD)	T_0	$2454508.9761^{+0.0002}_{-0.0002}$	days
Orbital Period	P	$1.091423^{+0.000003}_{-0.000003}$	days
Planet/Star Area Ratio	$(R_p/R_s)^2$	$0.0138^{+0.0002}_{-0.0002}$	
Transit Duration	t_T	$0.122^{+0.001}_{-0.001}$	days
Impact Parameter	b	$0.36^{+0.05}_{-0.06}$	R_*
Stellar Reflex Velocity	K_1	$0.226^{+0.004}_{-0.004}$	km s^{-1}
Center-of-Mass Velocity	γ	$19.0845^{+0.002}_{-0.002}$	km s^{-1}
Orbital Semimajor Axis	a	$0.0229^{+0.0008}_{-0.0008}$	AU
Orbital Inclination	I	$83.1^{+1.4}_{-1.1}$	deg
Orbital Eccentricity	e	$0.049^{+0.015}_{-0.015}$	
Longitude of Periastron	ω	-74^{+13}_{-10}	deg
Stellar Mass	M_*	$1.35^{+0.14}_{-0.14}$	M_\odot
Stellar Radius	R_*	$1.57^{+0.07}_{-0.07}$	R_\odot
Stellar Surface Gravity	$\log g_*$	$4.17^{+0.03}_{-0.03}$	cgs
Stellar Density	ρ_*	$0.35^{+0.03}_{-0.03}$	ρ_\odot
Planet Radius	R_p	$1.79^{+0.09}_{-0.09}$	R_J
Planet Mass	M_p	$1.41^{+0.10}_{-0.10}$	M_J
Planetary Surface Gravity	$\log g_p$	$2.99^{+0.03}_{-0.03}$	cgs
Planet Density	ρ_p	$0.24^{+0.03}_{-0.02}$	ρ_J
Planet Temperature ($A = 0, F = 1$)	T_{eq}	2516^{+36}_{-36}	K

taken as part of the Canarian Observatories International Time Programme. Three consecutive 1800 s exposures were taken using the yellow filter and grism. The spectra were binned 2×1 in the spatial direction at the time of observation to reduce the readout time. A slit width of $0/8$ was adopted which resulted in a spectral resolution of $R \sim 57,000$. Calibration images, including bias frames, lamp flat-field frames, and thorium-argon arcs, were taken at the beginning of the night and used in processing the target spectra with the REDUCE echelle data reduction package (Piskunov Valenti 2002). Special care was taken to provide an accurate flat fielding of the data. The three individual reduced spectra were averaged on an order-by-order basis to produce a final merged spectrum which was then used in the determination of the stellar parameters described in Section 3.1.

3. ANALYSIS

3.1. Spectroscopic Analysis

Three spectra of WASP-12 were derived from observations with the SARG, SOPHIE, and IDS spectrographs. Each independent spectrum was compared with synthetic spectra to determine the effective temperature T_{eff} , gravity $\log g$, metallicity, $[M/H]$, and projected stellar rotation $v \sin i$ of WASP-12. Our spectral synthesis technique closely follows the procedure of Valenti Fischer (2005; hereafter VF05), and a detailed description can be found in Stempels et al. (2007).

Two additional parameters, microturbulence and macroturbulence, are incorporated into the spectral synthesis to characterize turbulent mixing and convection in the upper layers of stellar atmospheres (Gray 1988). Their chosen values affect the derived stellar properties such that microturbulence anticorrelates strongly with metallicity, and macroturbulence affects the line broadening, and therefore the $v \sin i$ measurement. In our spectral synthesis, we closely follow VF05, so that our results can be compared directly with this extensive spectroscopic analysis of planet-hosting stars. For the microturbulence, we adopt their value of $v_{\text{mic}} = 0.85 \text{ km s}^{-1}$, but we note that other empirical studies of main-sequence F-stars suggest higher values for v_{mic} (see Montalbán & D'Antona 2007). For the macroturbulence, we use the empirical linear relation with temperature provided in VF05 to derive a value of $v_{\text{mac}} = 4.8 \text{ km s}^{-1}$. However, larger values are not excluded for hot stars like WASP-12. This is due to the difficulty in accurately measuring macroturbulence for early-type stars where rotational broadening typically dominates the line widths. Furthermore, only 79 stars in the VF05 sample have $T_{\text{eff}} \geq 6200 \text{ K}$, so the empirical relation is not very well defined in this regime.

We used the SARG data to derive our best measurement of the parameters of the host star. This spectrum is of high resolution and good quality with no known residual instrumental features. Four spectral regions (shown in Figure 5) were selected for the fit because they are particularly sensitive to one or more of the parameters we aim to derive. A simultaneous fit to these four regions of the spectrum yielded a $T_{\text{eff}} = 6290 \text{ K}$, $\log g = 4.38$, and $[M/H] = 0.30$. The line broadening was equivalent to that of the spectral resolution, therefore we were only able to derive an upper limit on the rotational broadening of $v \sin i < 2.2 \text{ km s}^{-1}$. This is derived by subtracting (in quadrature) the estimated value of macroturbulence (4.8 km s^{-1}) from the width of the smallest resolvable resolution element (5.3 km s^{-1} at $R = 57,000$). A comparison of the observed and best-fitting model spectra is shown in Figure 5, and the final stellar parameters are listed in Table 1. We derive uncertainties on these properties based on the range of values measured from the additional analysis of the IDS and SOPHIE data.

In the SOPHIE spectrum, we simultaneously fit the same four spectral regions given above and find $T_{\text{eff}} = 6175 \text{ K}$, $\log g = 4.36$, and $[M/H] = 0.15$. We also measure a $v \sin i = 4.5 \text{ km s}^{-1}$. Again, we believe this value is only an upper limit. The IDS spectrum spanned the region of $H\alpha$ and surrounding metal lines. In this region, there are no strongly gravity-sensitive features, therefore, we fixed the $\log g = 4.36$, which was determined from the SOPHIE observations, and solved for the stellar temperature, $T_{\text{eff}} = 6495 \text{ K}$, and metallicity, $[M/H] = 0.16$. The resolution was too low to measure $v \sin i$.

In summary, we made three independent measurements of the properties of WASP-12 by comparing spectroscopic observations of the star to model spectra. In all three analyses,

we find that WASP-12 is a hot, slowly rotating, metal-rich, dwarf star. We adopt the results from the analysis of the SARG spectrum as our final values for the parameters of WASP-12 and the uncertainties on the stellar parameters from the range of values that were determined in the three different analyses.

3.2. Deriving Planet and Host-Star Parameters

The multiband light curves and RV curve of WASP-12 were analyzed simultaneously in a Markov chain Monte Carlo (MCMC)-based routine designed specifically to solve the multivariate problem of transiting star–planet systems. The routine is described in detail in Collier Cameron et al. (2007) and Pollacco et al. (2008). The results of the box least-squares analysis of the SuperWASP photometric data (described in Section 2.1) provide an initial estimate of the light-curve parameters. We also initially assume an eccentricity of 0.02, a systemic RV equal to the mean of the velocity data, and a velocity amplitude derived by fitting a sinusoidal velocity variation to the observed RVs by minimizing χ^2 . To derive a first guess for the stellar mass, we interpolate the supersolar metallicity ($Z = 0.03$, $[M/H] = 0.2$), zero-age main sequence (ZAMS) temperature–mass relation from Girardi et al. (2000) at the stellar temperature derived in the previous section, $T_{\text{eff}} = 6300 \text{ K}$. We adopt a stellar mass of $1.28 M_{\odot}$ as the initial value for this parameter.

Via the MCMC approach, the routine repeatedly adopts trial parameters until it converges on the set of values which produce the best model velocity curve and model light curves. The model light curves are generated from the analytic transit formulae found in Mandel & Agol (2002; adopting the small-planet approximation) and using the limb darkening coefficients for the appropriate photometric filters from Claret (2000, 2004). The sum of the χ^2 for all input data curves with respect to the models is the statistic used to determine goodness of fit. The routine also produces 1σ uncertainties on all the parameters.

3.2.1. Evolutionary Status of the Host Star

We ran the MCMC code initially using the SuperWASP light curve, the B - and z -band follow-up photometry, and the SOPHIE RV curve as input data sets. We ran the code without imposing the main sequence prior on the overall χ^2 statistic. This is not unreasonable for a late-F star which, according to the theoretical models, has a main-sequence lifetime of $\lesssim 1 \text{ Gyr}$. We then determined the evolutionary status of the host star using the results of this run to assess whether this was a reasonable assumption.

First, we examined the lithium abundance in WASP-12 as a possible age indicator. In the SARG spectrum, there is no absorption detected in the Li I line located at 6708 \AA . The IDS spectrum shows a broad, very shallow absorption feature at this position; however, due to the lack of detection in the SARG spectrum, we suspect that the feature is due to noise or blending with other absorption lines (e.g., Fe I at 6707.44 \AA). This lack of Li is consistent with low levels found in old open clusters, like M 67 ($\sim 4 \text{ Gyr}$), for a 6300 K star (Sestito & Randich 2005); however, a precise age determination cannot be derived for the star from this observation.

Next, we compare the structure and temperature of the star to the supersolar metallicity stellar evolution models of Girardi et al. (2000) to constrain the age. We use the $[M/H] = 0.2$ ($Z = 0.03$) tracks which are consistent with the measured metallicity of WASP-12, given the uncertainty on this parameter. Figure 6 shows a modified Hertzsprung–Russell

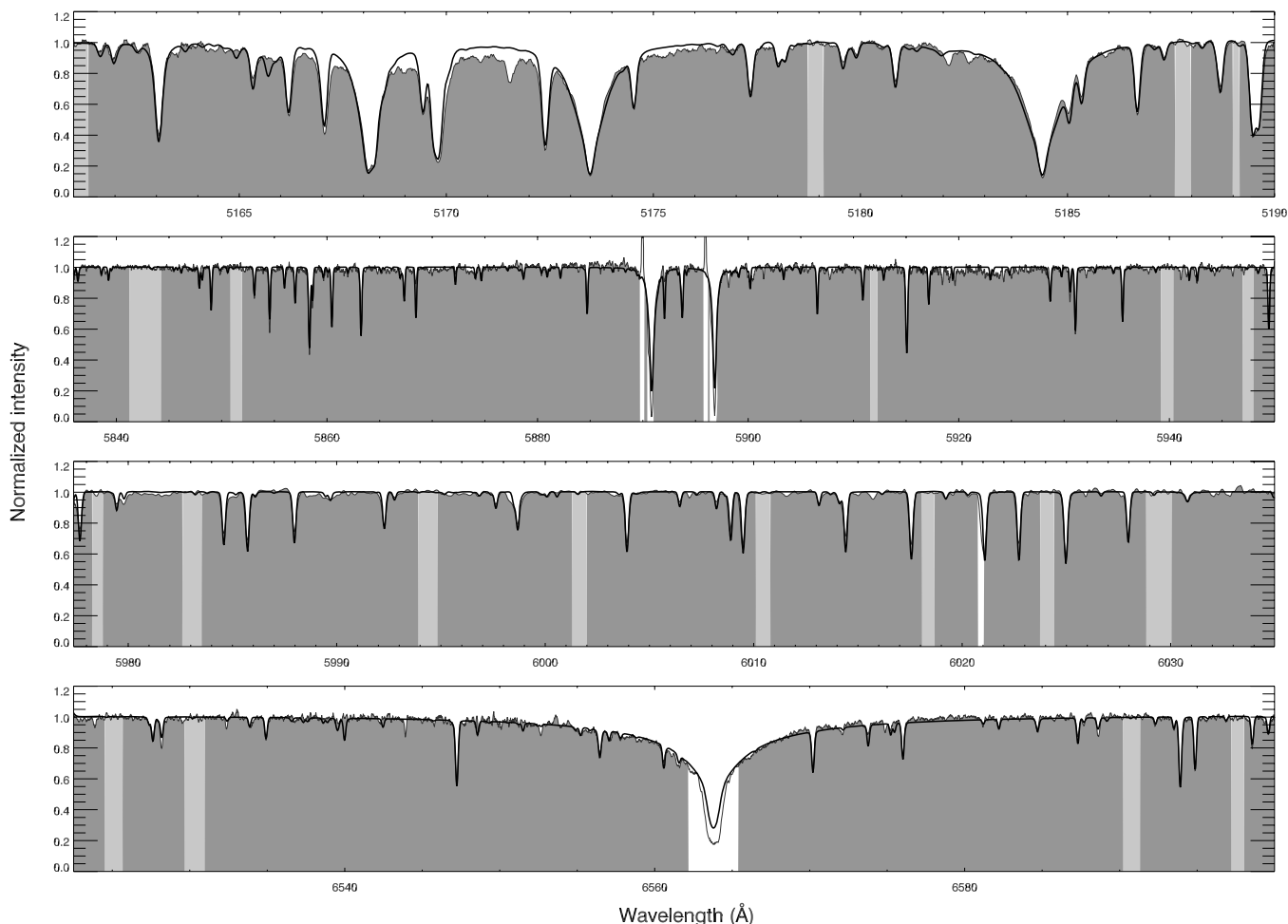


Figure 5. Observed SARG spectrum (gray) overlaid by the best-fitting theoretical model spectrum (solid black line). The top panel shows the region around the Mg b triplet (5160–5190 Å), the second panel is the region around the Na I D doublet (5850–5950 Å), the third panel shows the region from 6000 to 6210 Å with a large number of metal lines, and the bottom panel is the region around the H α line (6520–6600 Å). These regions are modeled simultaneously with spectral synthesis to derive the parameters of the host star. The light gray regions of the spectrum are used to determine the continuum. Note that narrow telluric emission features are present in the second panel at the rest wavelength of the Na I doublet feature.

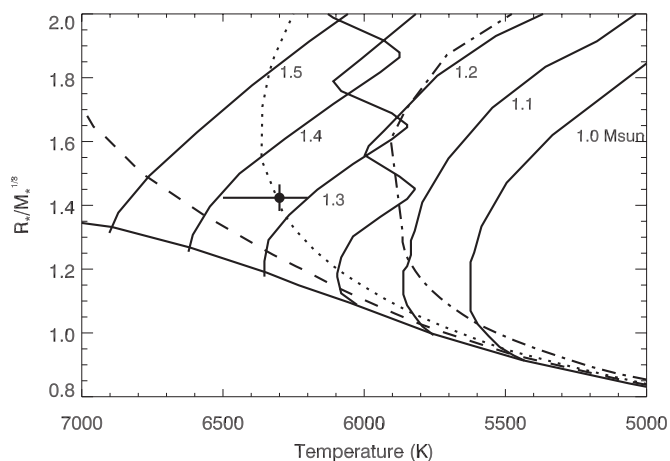


Figure 6. $R_*/M_*^{1/3}$ in solar units vs. effective temperature. WASP-12 is the large solid circle. Evolutionary mass tracks (solid lines with adjacent numbers labeling the mass of that line) and isochrones (100 Myr, solid; 1 Gyr, dashed; 2.0 Gyr, dotted; 5.0 Gyr, dot-dashed) from Girardi et al. (2000) for $Z = 0.03$ are plotted for comparison to the WASP-12 parameters.

(H–R) diagram comparing the host star to the theoretical mass tracks and isochrones. Here, we plot the inverse cube root of

the stellar density, $R_*/M_*^{1/3}$, in solar units versus the stellar temperature. We choose to compare the data to the models in this parameter space since the quantity, $R_*/M_*^{1/3}$, unlike R_* or luminosity, is purely observational and is measured directly from the light curve. In addition, it is completely independent of the temperature determined from the spectrum.

The results of the initial MCMC run provided a measurement of the mean stellar density. We converted the density to $R_*/M_*^{1/3}$ in solar units, and generated the same property from the mass and $\log g$ values in the models. We then interpolated in the $R_*/M_*^{1/3} - T_{\text{eff}}$ plane to determine the mass and age of WASP-12. We interpolated linearly along two consecutive mass tracks to generate an equal number of age points between the ZAMS and the coolest point at the end of core hydrogen burning. We then interpolated between the mass tracks along equivalent evolutionary points to find the mass and age from the models that best match the stellar properties derived from the MCMC code and the spectral synthesis. According to these particular tracks, the large value for $R_*/M_*^{1/3}$ indicates that the star has evolved off the ZAMS, but has yet to reach the shell hydrogen burning stage. It is in a position in the diagram which give it a mass, $M_* = 1.33 \pm 0.05 M_\odot$ and an age of $2.0_{-0.8}^{+0.5}$ Gyr. To check the accuracy and precision of this result, we compared the star to a

second set of stellar evolution models. When interpolating the $Z = 0.03$ tracks by Yi et al. (2003), we find a similar result. The position of the star in the $R_*/M_*^{1/3}-T_{\text{eff}}$ gives an age of 2.4 Gyr and a mass of $1.38 M_{\odot}$.

We investigated using the rotation period of the star which allows for constraining the age based on the expected spin-down timescale. The slow rotational period argues for an old age, however with only an upper limit on the $v \sin i$ we are unable to derive an age estimate using the gyrochronology technique (Barnes 2007).

The three age-dating techniques discussed all suggest that WASP-12 is several Gyr old; however, the stellar evolution models provide the only definitive estimate of the age. Therefore, we adopt a final age for WASP-12 of $\tau = 2 \pm 1$ Gyr. We have increased the uncertainty to include the error in metallicity and the systematics in the stellar evolution models.

3.2.2. Final Determination of Planet and Host-Star Parameters

After determining the evolutionary status of the host star and estimating the stellar mass from the evolutionary models, we ran the MCMC code a second time. We did not impose the main-sequence mass–radius prior, since the star has evolved off the ZAMS. Furthermore, we adopted an initial estimate for the stellar mass of $1.33 M_{\odot}$ from the comparison to the theoretical tracks.

In addition, during the SOPHIE observing run, we attempted to detect the Rossiter–McLaughlin effect by taking six consecutive measurements of the target during and just after the expected transit. We see no evidence for this effect in the data which confirms a small $v \sin i$ for WASP-12, and is consistent with the upper limit on the projected rotational velocity derived from the spectral synthesis. We do not currently use the in-transit RV data to derive an independent measurement of $v \sin i$, however, we do not wish for this sequence of observations, comprising 1/4 of our RV measurements, to bias the fit to the system orbital parameters. A small, but systematic zero-point offset in these data could affect the final results. Therefore, we treated the six data points taken in sequence on the same night as a different data set during the fitting which allows them to have a slight zero-point offset compared to all the other data points. The resulting zero-point offset is only 0.014 m s^{-1} .

The results of the final fit to the light curves and velocity curve using the SOPHIE RV data, the SuperWASP photometry, the Liverpool Telescope z -band, and the Tenagra B -band data are given in Table 3 with their 1σ uncertainties. The model light curves in each band are overplotted on the phase-folded data in Figure 2, and the model RV curve is shown in Figure 4. In the analysis, we find that WASP-12b is a low-density planet ($\sim 0.24\rho_J$) with a mass approximately 40% larger than Jupiter in a 1 day orbit around a hot, metal-rich late-F star which is evolving off the ZAMS.

We closely examined the most fundamental fitted parameters (depth, width, and impact parameter) which are used to describe the shape of the transit itself and find the model to be a good match to the data. We do note that the impact parameter, b , which is determined by the shape of the ingress and egress, is difficult to measure precisely without exceptionally good photometry. Furthermore, this parameter strongly influences the stellar radius and thus the planet radius through the depth measurement. Since the impact parameter has such a subtle effect on the light curve, but a large effect on the resulting parameters, we calculate an absolute lower limit on the planet radius by running the MCMC code with the impact parameter fixed to zero ($b = 0$ model).

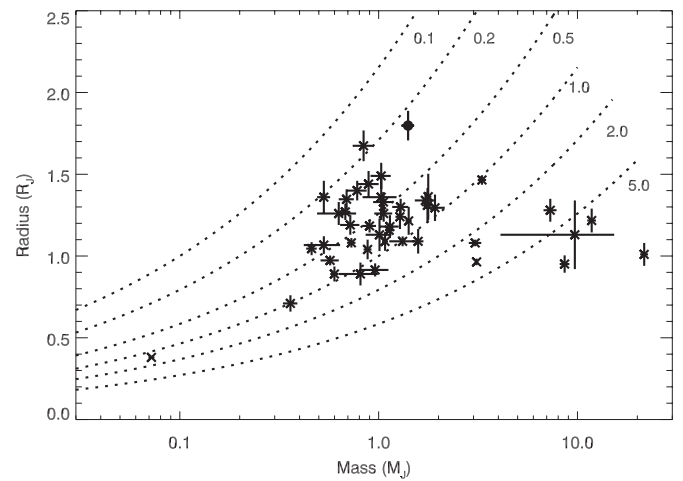


Figure 7. Mass vs. radius of all transiting planets which have published masses and radii. The data were obtained from the exoplanet encyclopedia (<http://exoplanet.eu>). WASP-12b is the solid black circle. Lines of constant planet density are overplotted (dotted) in units of Jupiter density.

The $b = 0$ model has a greater χ^2 compared to the overall best-fitting model by 15, which is significant, but the effect on the light curve is very subtle. However, when comparing the results of the $b = 0$ model to the overall best fit, we find a stellar radius of $R_{*,b=0} = 1.46 R_{\odot}$ compared to $R_* = 1.57 R_{\odot}$ and a planet radius of $R_{\text{pl},b=0} = 1.63 R_J$ compared to $R_{\text{pl}} = 1.79 R_J$.

4. DISCUSSION

WASP-12b is a unique transiting planet with the most apparent feature being the very large observed radius ($1.79 R_J$). The planet has a mean density only 24% that of Jupiter, making it a member of the growing class of transiting gas giants which all have particularly large radii. Figure 7 shows the position of WASP-12b among the other published transiting planets in the mass–radius plane. The structure of these planets, including HD 209458b and WASP-1b, cannot be explained through simple, isolated planet-formation models, and a great deal of recent theoretical work has gone into determining the mechanism or mechanisms causing their large sizes. It is clear that the external environment (stellar irradiation, tidal forces), the internal properties (heavy element abundance, clouds/hazes, day–night heat transfer, core mass), and the evolutionary state (age) can all affect a planet’s radius (Guillot Showman 2002; Bodenheimer et al. 2003; Fortney et al. 2007, 2008; Burrows et al. 2007, 2008a, 2008b; Jackson et al. 2008).

WASP-12b is the most heavily irradiated planet yet detected. With a host-star luminosity, $L = 3.48 L_{\odot}$, the planet experiences an incident flux at its substellar point of $F_p = 9.03 \times 10^9 \text{ erg cm}^{-2} \text{ s}^{-1}$, which is twice the stellar flux experienced by OGLE-TR-56b or OGLE-TR-132b, the next most highly irradiated planets (Torres et al. 2004; Burrows et al. 2007). This intense stellar radiation results in an equilibrium temperature, $T_{\text{eq}} = 2516((1 - A)/F)^{0.25} \text{ K}$, where A is the fraction of absorbed flux and F is the fraction of the planet’s surface that emits at T_{eq} . Although Jupiter has an absorbing fraction, $A = 0.28$ (Taylor 1965), existing evidence suggests that hot Jupiters have much lower albedos. For example, high-precision optical photometry of HD 209458b gives a geometric albedo of only 4% (Rowe et al. 2007).

It is clear from the detailed modeling of hot Jupiters (Bodenheimer et al. 2003; Fortney et al. 2007; Burrows et al.

2007) that increased incident stellar radiation will lead to an increase in the planet radius by inhibiting its contraction. This is a function of stellar mass and age, and less-massive planets are more affected by the star's radiation in this regard. The extremely irradiated case of the relatively massive WASP-12b planet ($M_p = 1.41 M_J$) at an age of ~ 2 Gyr is outside the range of situations presented in these papers, however, Fortney et al. (2007) give a radius of $1.248 R_J$ for an object similar to WASP-12b (1 Gyr old, $1.46 M_J$), but at a distance of 0.02 AU from a solar luminosity star. In the context of the models, the incident radiation from WASP-12 would be equivalent to putting this simulated planet at a distance of ~ 0.01 AU from a solar luminosity star. Despite WASP-12b being more intensely irradiated than the simulated planet of the same age and mass, it is difficult to see how stellar irradiation alone could result in the observed radius of $R_{pl} = 1.79 R_J$ (or even the absolute minimum radius of $R_{pl,b=0} = 1.63 R_J$) in a planet as massive as WASP-12b.

Burrows et al. (2007) show how enhancing the atmospheric opacities of extrasolar planets also results in increased radii by maintaining the heat and entropy stored in the cores over longer timescales. In their model, metallicity is used as a proxy for atmospheric heavy element abundance and thus opacity. Employing an abundance of 10 times solar allows the authors to fit the radii of the largest planets without adding any additional internal heat sources. It is very likely that WASP-12b has a supersolar atmospheric heavy element abundance, given the supersolar metallicity of the host star. Furthermore, according to the models of Fortney et al. (2008), WASP-12b should be in the class of highly irradiated, hot planets (pM class) in which high-altitude molecular hazes of TiO and VO (condensation temperature, $T = 1670$ K) absorb strongly at optical wavelengths resulting in larger radii. For WASP-12, measuring the primary and secondary eclipse depths as a function of wavelength and obtaining precise out-of-eclipse photometry will allow for investigating the presence of a high altitude absorbing population in the planet's atmosphere.

Although Burrows et al. (2007) do not calculate a model specifically for WASP-12b, they are able to reproduce a $1.30 R_J$, $1.29 M_J$, 2.5 Gyr old planet (OGLE-TR-56b). It will be interesting to see if a complete modeling of the extreme environmental conditions of WASP-12b including stellar irradiation, increased heavy-element abundance, and high altitude hazes can produce a sufficiently large planet radius to match the observed value.

If WASP-12b's large radius cannot be explained by increasing the atmospheric opacity or other atmospheric phenomena, an additional source of internal energy will be required to explain the observations. Dissipation of tidal energy is a possible contributor. The timescale for circularization of the WASP-12b orbit is most likely very short, but the best model fit to the observed RV and light curves produces a nonzero eccentricity of $e = 0.049_{-0.015}^{+0.015}$. Using the formalism for the circularization timescale taken originally from Goldreich Soter (1966) and provided in Bodenheimer et al. (2003), we find

$$\tau_{\text{circ}} = 3.2 \frac{Q_p}{10^6} \text{ Myr},$$

which is much shorter than the 2 Gyr age of WASP-12, when Q_p the tidal dissipation constant for the planet, is given the nominal value of 10^6 .

The nonzero eccentricity detection is barely a 3σ result, however, if after further observations, the detection persists, either the eccentricity must be continuously pumped by an outer planet or WASP12b's tidal dissipation constant must be significantly

larger than the typically adopted value (10^6). Since, the presence of an additional planet should be detectable via long-term RV monitoring, these two scenarios are distinguishable and thus this system might allow detailed constraints to be placed on Q_p , an important, but difficult to measure, parameter. Additionally, if a second planet is causing a nonzero eccentricity, the amount of internal tidal heating that must be dissipated is of the order of $5 \times 10^{28} (10^6 / Q_p) \text{ erg s}^{-1}$. This is a large amount of energy (2 orders of magnitude greater than what is calculated by Bodenheimer et al. 2003 for HD 209458b) which would have a significant effect on the radius of the planet.

WASP-12b is the hottest and largest transiting exoplanet yet detected. It has a mass, $M_{pl} = 1.41 M_J$, radius, $R_{pl} = 1.79 R_J$, and equilibrium planet temperature, $T_{\text{eq}} = 2516$ K. The planet orbits a bright late-F star with a temperature, $T_{\text{eff}} = 6300$ K and radius, $R_* = 1.57 R_{\odot}$. The host star has significantly enhanced metallicity over solar is evolving off the ZAMS, and has an age of ~ 2 Gyr. Additional follow-up observations of this exciting planet will address some of the most pressing questions in exoplanet research, in particular, what mechanism or mechanisms are causing the large observed radii of some hot Jupiters and what effect does the stellar irradiation and stellar metallicity have on the atmospheric and structural properties of close-in gas giant planets.

The SuperWASP Consortium consists of astronomers primarily from the Queen's University Belfast, St. Andrews, Keele, Leicester, The Open University, Isaac Newton Group La Palma, and Instituto de Astrofísica de Canarias. The SuperWASP Cameras were constructed and operated with funds made available from Consortium Universities and the UK's Science and Technology Facilities Council. SOPHIE observations have been funded by the Optical Infrared Coordination Network. The data from the Liverpool and NOT telescopes were obtained under the auspices of the International Time of the Canary Islands. We extend our thanks to the staff of the ING and OHP for their continued support of SuperWASP-N and SOPHIE instruments. The radial velocity observations have been funded by the Optical Infrared Coordination Network (OPTICON), a major international collaboration supported by the Research Infrastructures Programme of the European Commissions Sixth Framework Programme. This paper was based in part on observations made with the Italian Telescopio Nazionale Galileo (TNG) operated on the island of La Palma by the Fundación Galileo Galilei of the INAF (Istituto Nazionale di Astrofisica) at the Spanish Observatorio del Roque de los Muchachos of the Instituto de Astrofísica de Canarias. The Liverpool Telescope is operated on the island of La Palma by Liverpool John Moores University in the Spanish Observatorio del Roque de los Muchachos of the Instituto de Astrofísica de Canarias with financial support from the UK Science and Technology Facilities Council.

REFERENCES

- Baranne, A., et al. 1996, *A&AS*, **119**, 373
 Barnes, S. 2007, *ApJ*, **669**, 1167
 Bodenheimer, P., Laughlin, G., & Lin, D. N. C. 2003, *ApJ*, **592**, 555
 Bouchy, F., & The Sophie Team 2006, in Tenth Anniversary of 51 Peg-b: Status of and Prospects for Hot Jupiter Studies, ed. L. Arnold, F. Bouchy, & C. Moutou (Paris: Frontier Group), 319
 Brown, T. M., Charbonneau, D., Gilliland, R. L., Noyes, R. W., & Burrows, A. 2001, *ApJ*, **552**, 699
 Burrows, A., Budaj, J., & Hubeny, I. 2008a, *ApJ*, **678**, 1436
 Burrows, A., Ibgui, L., & Hubeny, I. 2008b, *ApJ*, **682**, 1277

- Burrows, A., Hubeny, I., Budaj, J., & Hubbard, W. B. 2007, *ApJ*, **661**, 502
- Christian, D. J., et al. 2009, *MNRAS*, **392**, 1585
- Claret, A. 2000, *A&A*, **363**, 1081
- Claret, A. 2004, *A&A*, **428**, 1001
- Collier Cameron, A., et al. 2006, *MNRAS*, **373**, 799
- Collier Cameron, A., et al. 2007, *MNRAS*, **380**, 1230
- Fortney, J. J., Lodders, K., Marley, M. S., & Freedman, R. S. 2008, *ApJ*, **678**, 1419
- Fortney, J. J., Marley, M. S., & Barnes, J. W. 2007, *ApJ*, **659**, 1661
- Girardi, L., Bressan, A., Bertelli, G., & Chiosi, C. 2000, *A&AS*, **141**, 371
- Goldreich, P., & Soter, S. 1966, *Icarus*, **5**, 375
- Gray, D. F. 1988, *Lectures on Spectral-Line Analysis: F, G, and K Stars* (Ontario: Arva)
- Guillot, M., & Showman, A. P. 2002, *A&A*, **385**, 156
- Jackson, B., Greenberg, R., & Barnes, R. 2008, *ApJ*, **678**, 1396
- Kovács, G., Zucker, S., & Mazeh, T. 2002, *A&A*, **391**, 369
- Mandel, K., & Agol, E. 2002, *ApJ*, **580**, L171
- Montalbán, J., & D'Antona, F. 2007, in *IAU Symp. 239, Convection in Astrophysics*, ed. F. Kupka, I. Roxburgh, & K. Chan (Dordrecht: Kluwer), 320
- Pepe, F., et al. 2005, *The Messenger*, **120**, 22
- Piskunov, N. E., & Valenti, J. A. 2002, *A&A*, **385**, 1095
- Pollacco, D., et al. 2006, *PASP*, **118**, 1407
- Pollacco, D., et al. 2008, *MNRAS*, **385**, 1576
- Pont, F., Zucker, S., & Queloz, D. 2006, *MNRAS*, **373**, 231
- Queloz, D., et al. 2001, *A&A*, **379**, 279
- Rowe, J. F., et al. 2008, *ApJ*, **689**, 1345
- Sestito, P., & Randich, S. 2005, *A&A*, **442**, 615
- Skrutskie, M. F., et al. 2006, *AJ*, **131**, 1163
- Steele, I. A., et al. 2004, *Proc. SPIE*, **5489**, 679
- Stempels, H. C., et al. 2007, *MNRAS*, **379**, 773
- Stetson, P. 1987, *PASP*, **99**, 191
- Taylor, D. J. 1965, *Icarus*, **4**, 362
- Torres, G., Konacki, M., Sasselov, D. D., & Jha, S. 2004, *ApJ*, **609**, 1071
- Valenti, J. A., & Fischer, D. 2005, *ApJS*, **159**, 141
- West, R. G., et al. 2008, *arXiv:0809.4597*
- Yi, S. K., Kim, Y.-C., & Demarque, P. 2003, *ApJS*, **144**, 259
- Zacharias, N., Monet, D. G., Levine, S. E., Urban, S. E., Gaume, R., & Wycoff, G. L. 2004, *BAAS*, **36**, 1418